

## Z and W production in the forward region

---

**Ronan WALLACE\*** on behalf of the LHCb Collaboration.

*University College Dublin (IE)*

*E-mail:* [ronan.wallace@cern.ch](mailto:ronan.wallace@cern.ch)

Measurements of electroweak boson production cross-sections are presented. The results include decays to both muons and electrons, as well as production with at least one b-jet. The data were recorded by the LHCb detector during  $pp$  collisions at centre-of-mass energies of 7 and 8 TeV, and correspond to integrated luminosities of 1.0 and 2.0  $\text{fb}^{-1}$ . The inclusive cross-sections are measured with total uncertainties as low as 2% and the results are in good agreement with theoretical predictions at next-to-next-to-leading order in perturbative quantum chromodynamics. Ratios of the production cross-sections of electroweak bosons are presented and a precise test of the Standard Model is provided by the measurement of the ratio

$$\frac{\sigma_{W^+ \rightarrow \mu^+ \nu_\mu} + \sigma_{W^- \rightarrow \mu^- \bar{\nu}_\mu}}{\sigma_{Z \rightarrow \mu^+ \mu^-}},$$

where the uncertainty due to luminosity cancels. These ratio measurements are sensitive to the parameterisation of parton distribution functions; the data display preferences for some over others. An interpretation of these preferences is discussed.

*XXIII International Workshop on Deep-Inelastic Scattering  
27 April - May 1 2015  
Dallas, Texas*

---

\*Speaker.

## 1. Introduction

Measurements of the total and differential cross-sections for the production of electroweak bosons in  $pp$  collisions test the Standard Model (SM) and provide constraints on parton density functions (PDF) of the proton. Theoretical predictions for these cross-sections are available at next-to-next-to-leading order (NNLO) in perturbative quantum chromodynamics [1] [2], for which the dominant uncertainty is due to the PDF uncertainty. This uncertainty depends on the scale of the process,  $Q^2$ , as well as the longitudinal momentum fraction of the parton,  $x$ . Due to the forward geometry of LHCb, production of electroweak bosons is predominantly due to high- $x$  valence-quark and low- $x$  sea-quark annihilation, while jets in the final-state are indicative of the quark-gluon production mechanism. The PDFs in the high- $x$  region are relatively well constrained by deep inelastic scattering data. Electroweak boson production data from LHCb has played a role in constraining the d-quark distributions in this high- $x$  region [3]. It also has potential to provide constraints on the low- $x$  ( $\sim 10^{-4}$ ) sea at high  $Q^2$  ( $\sim 10^4$  GeV<sup>2</sup>). Ratios of the  $W$  and  $Z$  cross-sections provide precise tests of the SM, as the sensitivity to the PDFs in the theoretical calculations is reduced and many of the correlated experimental uncertainties cancel.

These proceedings discuss an update of electroweak boson production with subsequent decay to muons (see Refs. [4], [5]) with  $1 \text{ fb}^{-1}$  [6], an analysis of  $Z \rightarrow ee$  production similar to Ref. [7] but at  $\sqrt{s} = 8 \text{ TeV}$  with  $2 \text{ fb}^{-1}$  [8], and a new analysis,  $Z$ +b-jet production using  $1 \text{ fb}^{-1}$  of data at  $\sqrt{s} = 7 \text{ TeV}$  [9].

## 2. Selection

The  $Z$  candidates are selected by requiring two well reconstructed and oppositely charged leptons in the pseudorapidity range between 2.0 and 4.5 with transverse momentum  $p_T > 20 \text{ GeV}/c$ . The invariant mass of the dimuon combination is required to be between  $60 \text{ GeV}/c^2$  and  $120 \text{ GeV}/c^2$ , while the di-electron invariant mass needs to be greater than  $40 \text{ GeV}/c^2$ . The mass distributions of these candidates are shown in Figure 1. The largest remaining backgrounds in these

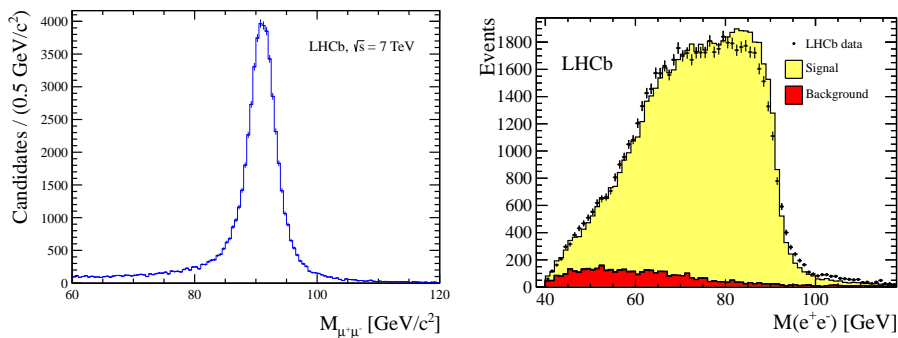


**Figure 1:** Invariant mass distribution of dimuon (left) and di-electron (right) candidates. The broad mass peak of di-electron candidates is due to bremsstrahlung.

samples are estimated using data-driven methods. The  $Z \rightarrow \mu\mu$  selection is very pure with 99.3%

signal. Semi-leptonic decays of B and D hadrons to high- $p_T$  muons are estimated by exploiting the fact that these muons are non-prompt and are accompanied by QCD activity. Two independent background enriched samples are constructed using the signal sample. The first requires both of the muons to have less than 70% of the total transverse momentum in a cone of radius 0.5 in  $\eta - \phi$  space around the muon track. The second requires the  $\chi^2/ndf$  for the dimuon vertex fit to be greater than 100. Both require a dimuon mass greater than  $40 \text{ GeV}/c^2$ . The resulting invariant mass distributions are fitted with an exponential form to determine the contribution in the signal mass window. Same-sign events are also used to quantify backgrounds. The  $\pi/K$  decay in flight and punch-through backgrounds to  $Z \rightarrow \mu\mu$  are expected to contribute equally in same-sign and opposite-sign pairs as is the early showering of hadrons faking electrons, the dominant background in the  $Z \rightarrow ee$  channel. This contribution is indicated in the right hand plot of Figure 1.

The  $W \rightarrow \mu\nu$  candidates are selected by requiring a well reconstructed muon with high transverse momentum  $20 < p_T < 70 \text{ GeV}/c$  in the pseudorapidity range between 2.0 and 4.5. Events with an additional opposite-sign muon with transverse momentum greater than  $2 \text{ GeV}/c$  are vetoed. To suppress muons from long-lived particles, the muon impact parameter is required to be less than  $40 \mu\text{m}$ . To suppress hadron misidentification, the energy of charged and neutral particles in a cone of radius 0.5 in  $\eta - \phi$  space around the candidate muon is required to be small. To determine

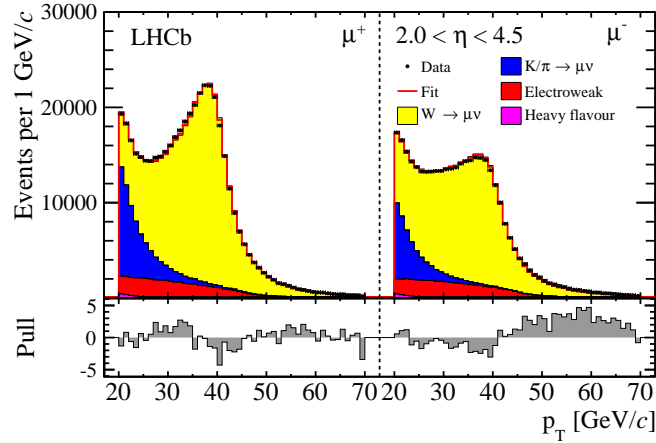


**Figure 2:** Template fit of lepton  $p_T$  distribution to  $W$  boson candidate sample.

the purity, signal and background templates are fitted to the  $p_T$  distribution of the muons as in Figure 2. The signal template normalisation is free to vary in each pseudorapidity bin in the fit. The  $Z \rightarrow \mu\mu$  background normalisation is fixed by scaling the number of  $Z$  events in data by the ratio of  $Z$  events with one lepton in the acceptance to  $Z$  events with two leptons in the acceptance, determined with simulation. Another significant background is decay in flight of  $\pi/K$  before the muon chambers. This template is determined by weighting the transverse momentum distribution of charged hadrons (calculated using events triggered by any LHCb trigger except the muon trigger) with the probability that the hadron decays to a muon. This probability is given by the fraction of tracks identified as muons in randomly triggered events. The normalisation in each bin is free to vary. Other simulated templates are used to model  $W \rightarrow \tau\nu$ ,  $Z \rightarrow \tau\tau$  and decays of B and D

hadrons.

The Z+b-jet selection is built on top of the  $Z \rightarrow \mu\mu$  selection, where in addition a jet with  $p_T > 20$  GeV/c in the pseudorapidity range between 2 and 4.5 is required. A particle-flow algorithm is used to build *anti*- $k_T$  jets with  $R=0.5$ , which are required to be separated from the muons in  $\eta - \phi$  space. The jets are flavour-tagged by requiring a secondary vertex within the jet consisting of either 2, 3, or 4 charged or neutral particles. The requirement of a flavour-tagged jet reduces the light- and c-jet contamination. The Z+b-jet fraction of these flavour-tagged events is extracted using a template fit to the corrected mass of the secondary vertex, shown in Figure 3. The corrected

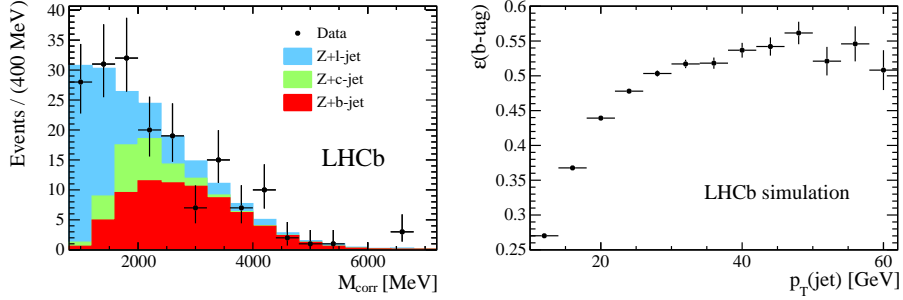


**Figure 3:** Corrected mass (left) and b-tagging efficiency (right).

mass is defined as  $M_{corr} = \sqrt{M^2 + p^2 \sin^2 \theta} + p \sin \theta$ , where  $M$  and  $p$  are the mass and momentum of the secondary vertex. The angle between the momentum of the secondary vertex and the vector between the interaction point and secondary vertex is  $\theta$ . This angle is used to infer a component of the missing energy at the secondary decay vertex. The corrected mass takes this component into account and is thus a better estimate (but still an underestimate) of the mass of the particle decaying at the secondary vertex. The efficiency of the flavour tagging algorithm is evaluated using Z+b-jet simulation and is shown in Figure 3 as a function of jet  $p_T$ .

### 3. Results

Inclusive differential cross-sections of  $W$  and  $Z$  are calculated for leptons with  $p_T > 20$  GeV/c and pseudorapidities between 2.0 and 4.5. In the case of the  $Z$ , the dimuon invariant mass must be between 60 and 120 GeV/c<sup>2</sup>. Cross-sections are calculated using the formula

$$\sigma = \frac{\rho N}{\epsilon \mathcal{L}} f_{FSR}. \quad (3.1)$$

Muon reconstruction efficiencies are determined from data using tag-and-probe methods. Corrections for detector occupancy thresholds in the trigger are also applied. These are represented by  $\epsilon$ . The purity of the sample is denoted by  $\rho$ , final-state QED radiation by  $f_{FSR}$ , and the integrated luminosity by  $\mathcal{L}$ . Results for electroweak boson cross-sections are summarised in Figure 4 where they are compared to the NNLO predictions of FEWZ [1] with various PDF sets [3], [10], [11] [12], [13], [14]. The precision of each measurement is  $\sim 2\%$ , which is dominated by the luminosity determination [15]. There is good agreement with the SM, which is also the case for the  $Z \rightarrow ee$  measurement. The ratios of these cross-sections are also displayed. The

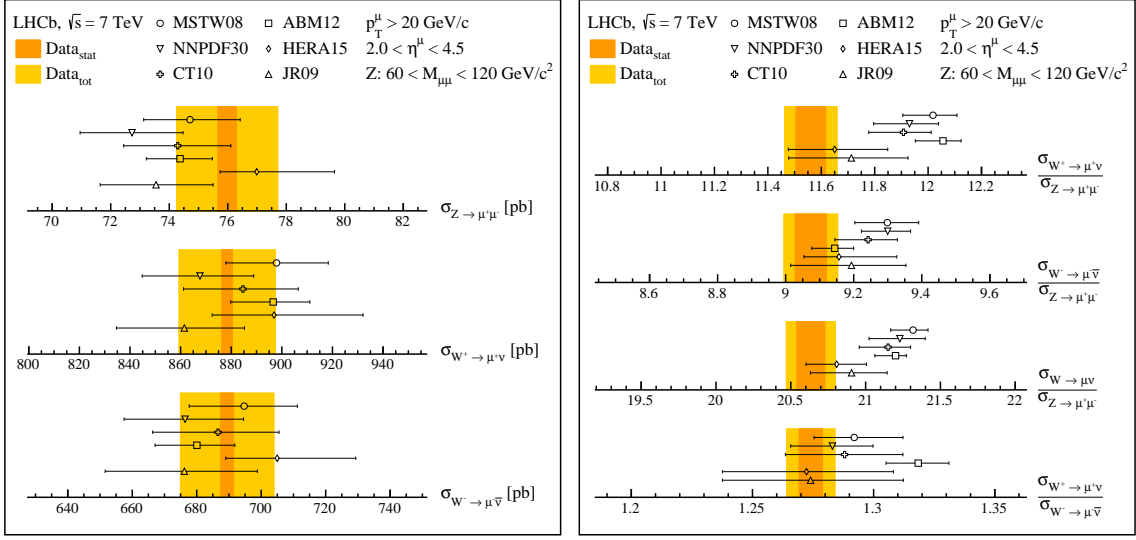


**Figure 4:** Summary of electroweak boson cross-section (left) and ratio (right) measurements.

largest uncertainty on the cross-sections, the luminosity, completely cancels in these ratios, as well as other correlated systematic uncertainties such as the proton beam energy [16]. The precision on the ratios varies between 0.8% and 0.9%. The total uncertainties on the theoretical predictions include uncertainties due to the PDFs, scale,  $\alpha_s$  and numerical integration. As stated above, the uncertainties on the predicted cross-sections due to PDFs are correlated, and the coefficients range between 0.54 and 0.99. Due to scale and  $\alpha_s$  uncertainties, the correlation coefficients are above 0.99. This ensures that the predicted ratios are determined to sub-percent level. The level of experimental and theoretical precision on these ratios makes these measurements an excellent test of both the SM and PDFs. The sensitivity to the choice of PDF is evident from Figure 4, particularly for ratios involving the Z boson cross-section. The cross-sections for Z+b-jet production for different jet  $p_T$  thresholds are shown in Figure 5. The data are compared to predictions from MCFM [17] configured with the MSTW08 PDF set [10], where there is good agreement.

#### 4. Discussion

The results displayed in Figure 4 merit further discussion. The cross-sections in the left hand panel show good agreement with predictions, but with the increased relative precision in the ratios of the right hand panel, there is some tension with certain individual PDF sets. If the spread of the predictions is taken into account, the data are in better agreement.

It is curious that the  $W^+/W^-$  predictions (apart from the ABM12 PDF [3]) overlap with the measurement, whereas the predictions involving the Z boson are systematically higher. If one looks carefully at the left hand panel of Figure 4, one can see that the central values for the W bosons are similar for measurement and theory, whereas the measured Z cross-section is higher than all but the HERA PDF [13]. In the forward region of LHCb, the  $W^+/W^-$  ratio is an approximate measurement of the u/d quark ratio at high- $x$  [18]. Since the measured and predicted  $W^+/W^-$

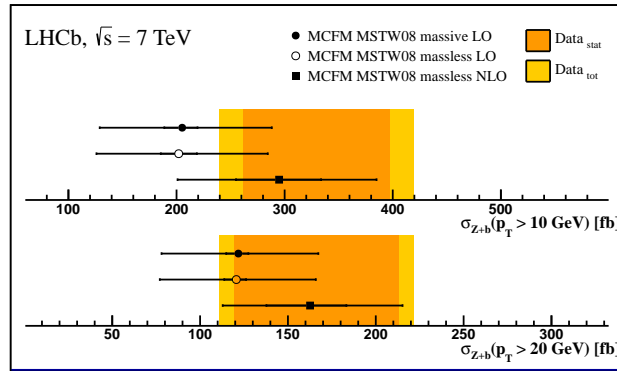


**Figure 5:** Z+b-jet cross-section for 10 GeV/c (top) and 20 GeV/c (bottom)  $p_T^{jet}$  thresholds.

ratios agree, whereas those involving the Z boson are in tension, it is natural to ask if these LHCb measurements are sensitive to the s-quark content of the proton.

The dimuon data from the CCFR [19] and NuTeV [20] experiments ( $\nu A \rightarrow \mu^+ \mu^- X$ ) favour a suppression of the s-quark sea with respect to the u- and d-quark sea. Initially, this suppression was set by hand in several PDF fits by imposing  $\kappa = 2s/(\bar{u} + \bar{d}) \approx 0.4 - 0.5$ . More recently, the s-quark parameterisation has been given more freedom in the fit. Some parameters are still fixed to control a suppression at low- $x$ , which is interpreted as the effect of a non-negligible s-quark mass [10], [12]. Such a suppression would effect production of Z bosons to a greater extent than W bosons on the basis that two  $g \rightarrow s\bar{s}$  splittings from the sea are more likely than one  $g \rightarrow s\bar{s}$  and one  $g \rightarrow c\bar{c}$ . Thus, a symmetric light-quark (u,d,s) sea as proposed by the ATLAS collaboration [21], could bring the predictions into better agreement with LHCb measurements. During the plenary session, the use of the CCFR and NuTeV dimuon data in global fits of parton distributions was questioned [22]. Intermediate interactions between the nucleon and c-quark make this data important for the extraction of nuclear PDFs, but the corrections required to recover proton PDFs are significant and induce uncertainties that are currently not under control. What is more, it has been shown that the s-quark PDF at low- $x$  is particularly sensitive to nuclear modification factors [23]. Preliminary investigations with PDF sets that do not include this  $\nu A$  data predict similar W cross-sections and a higher Z cross-section.

## References

- [1] Y. Li and F. Petriello, *Combining QCD and electroweak corrections to dilepton production in FEWZ*, *Phys. Rev. D* 86 094034 [hep-ph/1208.5967].
- [2] S. Catani *et. al.*, *Vector boson production at hadron colliders: A fully exclusive QCD calculation at NNLO*, *Phys. Rev. Lett.* 103 (2009) 082001 [hep-ph/0903.2120].
- [3] S. Alekhin and J. Blümlein and S. Moch, *The ABM parton distributions tuned to LHC data*, *Phys. Rev. D* 89 054028 [hep-ph/1310.3059].
- [4] The LHCb collaboration, *Inclusive W and Z production in the forward region at  $\sqrt{s} = 7$  TeV*, *JHEP* 06 (2012) 058 [hep-ex/1204.1620].

- [5] The LHCb collaboration, *Measurement of the forward W boson cross-section in pp collisions at  $\sqrt{s} = 7$  TeV*, *JHEP* **12** (2014) 079 [hep-ex/1408.4354v1].
- [6] The LHCb collaboration, *Measurement of the forward Z boson production cross-section in pp collisions at  $\sqrt{s} = 7$  TeV*, hep-ex/1505.07024.
- [7] The LHCb collaboration, *Measurement of the cross-section for  $Z \rightarrow e^+e^-$  production in pp collisions at  $\sqrt{s} = 7$  TeV*, *JHEP* **02** (2013) 106 [hep-ex/1212.4620].
- [8] The LHCb collaboration, *Measurement of forward  $Z \rightarrow e^+e^-$  production at  $\sqrt{s} = 8$  TeV*, *JHEP* **05** (2015) 109 [hep-ex/1503.00963v1].
- [9] The LHCb collaboration, *Measurement of the Z+b-jet cross-section in pp collisions at  $\sqrt{s} = 7$  TeV in the forward region*, *JHEP* **01** (2015) 064 [hep-ex/1411.1264].
- [10] A.D. Martin, W. J. Stirling, R.S Thorne and G. Watt, *Parton distributions for the LHC*, *Eur. Phys. J. C* **63** (2009) 189-2850 [hep-ph/0901.0002].
- [11] R.D. Ball *et. al.*, *A first unbiased global NLO determination of parton distributions and their uncertainties*, *Nucl. Phys. B* **838** (2010) 136-206 [hep-ph/1002.4407].
- [12] H.L. Lai *et. al.*, *New parton distributions for collider physics*, *Phys. Rev. D* **82** (2010) 074024 [hep-ph/1007.2241].
- [13] H1 and ZEUS collaborations, *Combined measurement and QCD analysis of the inclusive  $e^\pm p$  scattering cross sections at HERA*, *JHEP* **01** (2010) 109, [hep-ph/0911.0884].
- [14] P. Jimenez-Delgado and E. Reya, *Dynamical NNLO parton distributions*, *Phys. Rev. D.* **79** 074023 [hep-ph/0810.4274].
- [15] The LHCb collaboration, *Precision luminosity measurements at LHCb*, *JINST* **12** (2014) P12005, [hep-ph/1410.0149].
- [16] J. Wenninger, *Energy calibration of the LHC beams at 4 TeV*, CERN-ATS-2013-040, <http://cds.cern.ch/record/1546734>
- [17] J.M Campbell and R.K Ellis, *MCFM for the Tevatron and the LHC*, *Nucl. Phys. Proc. Suppl.* **205-206** (2010) 10 [hep-ph/1007.3492].
- [18] Martin, A. D. *et. al.*, *Parton distributions and QCD at LHCb*, *Proceedings DIS 2008*[hep-ph/0808.1847v1].
- [19] The CCFR collaboration, *Determination of the strange quark content of the nucleon from a next-to-leading-order QCD analysis of neutrino charm production*, *Z. Phys. C* **65** (1995) 189, [hep-ex/9406007].
- [20] The NuTeV collaboration, *Precise measurement of dimuon production cross-sections in muon neutrino Fe and muon anti-neutrino Fe deep inelastic scattering at the Tevatron*, *Phys. Rev. D* **64** (2001) 112006, [hep-ex/0102049].
- [21] The ATLAS collaboration, *Determination of the strange quark density of the proton from ATLAS measurements of the  $W \rightarrow lv$  and  $Z \rightarrow ll$  cross sections*, *Phys. Rev. Lett.* **109** (2012) 012001, [hep-ex/1203.4051].
- [22] A. Accardi, *Parton distributions from protons to nuclei*, Slides: <https://indico.cern.ch/event/341292/session/3/contribution/251/material/slides/0.pdf>
- [23] K. Kovarik *et. al.*, *A survey of heavy quark theory for PDF analyses*, *Proceedings of the Ringsberg Workshop*, [hep-ph/1201.1946v1].